JOURNAL OF PHYSICAL CHEMISTRY, 2025, Vol. 99, No. 1, c. 62–76

CHEMICAL KINETICS AND CATALYSIS

SYNTHESIS OF COMPLEX ALUMINA-COBALT SYSTEMS USING THERMALLY ACTIVATED GIBBSITE PRODUCT

A. V. Zhuzhgov[a], *, A. S. Gorkusha[a,b], E. A. Suprun[a], A. I. Lysikov[a,b], and L. A. Isupova[a]

[a] *Boreskov Institute of Catalysis of the Siberian Branch of the Russian Academy of Sciences, Novosibirsk, Russia*

Novosibirsk State University, Novosibirsk, Russia

Received April 11, 2024
Revised May 15, 2024
Accepted May 20, 2024

Abstract. Using the methods of X-ray phase, thermal, microscopic, adsorption, and chemical analyses, the possibility of obtaining high-percentage mixed alumina-cobalt spinels by hydrochemical treatment under room or hydrothermal conditions of powder suspensions of the product of centrifugal thermal activation of gibbsite in aqueous solutions of cobaltous nitrate is studied and shown. Thermal treatment of hydrochemical interaction products, viz. xerogels in the range of 350–850°C, is established to lead to the formation of Co_3O_4 and $CoAl_2O_4$ spinel phases with their different ratio depending on the synthesis conditions. Thus, hydrochemical treatment of suspensions at room temperature provides, after calcination, the predominant formation of the Co_3O_4 phase while hydrothermal treatment at 150°C leads to a deeper interaction of suspension components at the treatment stage, forming $CoAl_2O_4$ after thermal treatment. It is noted that the maximum content of spinel of $CoAl_2O_4$ type (90% according to H_2-TPR data) is observed for the hydrothermal product calcined at 850°C. The considered method is concluded to allow obtaining complex alumina-cobalt compounds with different phase ratio, reducing the number of initial reagents, preparation stages, completely excluding effluents, as well as reducing the total amount of nitrates by 75 wt%, as compared to the nitrate classical co-precipitation scheme.

Keywords: *gibbsite, product of centrifugal thermal activation of gibbsite, Co_3O_4 and $CoAl_2O_4$ spinels*

DOI: 10.31857/S004445372501O6e6

Aluminium-cobalt materials with a structure of layered double hydroxides (LDH), as well as products of their thermal decomposition, viz. aluminium-cobalt oxide systems (ACO) with a spinel structure (Co_3O_4/Al_2O_3, $CoAl_2O_4$, and Co_2AlO_4) are used in pharmaceuticals, bio-, photo- and electrochemistry. As modifiers of various polymer materials, for instance, to increase heat resistance of rubber [1–5]. In addition, ACO compounds in the nanodisperse state are used as materials for the production of high-performance supercapacitors (ionistors) [2, 6]. Complex multicomponent ACO compounds are used as catalysts in the Fischer-Tropsch synthesis process, as well as in various redox processes, for instance, low-temperature oxidation of carbon monoxide CO [7, 8]. Alumina-cobalt oxide catalyst systems, including those with a stoichiometric spinel structure of the so-called "normal" composition ($CoAl_2O_4$ with cobalt being ~33 wt%), are of considerable practical interest for use in hydrocarbon dehydrogenation/hydrogenation processes. They are used as catalysts for hydrogenation of furfural, acetone, conversion of methane, ethanol, and glycerol into valuable hydrocarbons and hydrogen, in the process of CO_2 methanation [9–13].

Hydrogen storage and transportation is one of the primary and significant directions in solving hydrogen energy tasks. For transportation and long-term storage of large volumes, hydrogen in the cryogenic liquid state (LH) at 21–24 K. However, when liquefying hydrogen of a "normal" composition, the components of which at 300 K exist in equilibrium at a ratio of 25% p-H_2 (*para*-hydrogen) and 75% o-H_2 (*ortho*-hydrogen), a slow reaction of ortho-para conversion (OPC) spontaneously occurs in the liquid phase. At the same the time thermal energy (about 1057 J/mol) is released, which exceeds own heat of liquid evaporation, which is 953 J/mol, leading to rapid uncontrolled losses of LH. It is estimated that the loss of hydrogen after its liquefaction in the first day is about 20%, and in four day there remains about half of the original volume. Long-term storage and, accordingly, long-distance transportation of liquid hydrogen is possible only if 95–98% of hydrogen molecules are transferred to the p-H_2 state. Thus, liquid *para*-hydrogen (we emphasize, the density of gas and liquid differ by

~800 times) provides an effective solution to storage and transportation tasks. During several months of liquid p-H_2 storage, losses do not exceed 10% of the initial volume. It is important to note that production of liquid hydrogen is a single process system including both the liquefaction stage and the stage of production and preliminary preparation of gaseous hydrogen, ensuring its purification from impurities, especially oxygen and nitrogen, in order to ensure explosion safety in hydrogen liquidizer systems. Contamination of liquid hydrogen with impurities of solid oxygen and nitrogen during operation of the liquefaction plant can lead to clogging of heat exchange tubes of reactors at temperature levels of 65–21 K. The process of after-treatment of hydrogen from oxygen impurities is carried out in reactors using stationary layers of special catalysts, which are high-percentage (with active component content of 30–40 wt%) systems based on aluminium and transition metals such as Co, Ni, Cu, Fe, and Cr, including in combination with each other in catalysts [14–21].

We consider the most common methods of preparing ACO. Various methods of preparing such materials are known in publications, characterized by both advantages and disadvantages. The most famous method of obtaining alumina-cobalt, as well as other single and multicomponent materials containing transition and non-transition metals, is the method of co-deposition (sol-gel technology) [22–25]. The disadvantages of this technology include the need to use a large amount of starting reagents (salts, acids, alkali), the formation of effluents at the stages of washing sediments from impurities, waste gases at the stages of drying and thermal treatment that are, in turn, required to be disposed.

The method of impregnation with solutions of salts of various metals, including cobalt, by moisture capacity of pre-prepared carriers based on aluminium oxides or their hydroxide precursors, among which pseudo-boehmite, boehmite, bayerite, as well as their mixtures, are widespread [9, 26]. The moisture capacity impregnation method limits the concentration of active component introduced into the pores of the carrier due to the moisture absorption limit of the carrier itself and the solubility of salts in the impregnating aqueous solutions.

Mechanochemical methods of preparation of alumina-cobalt systems [27–29] are used, which consist in preliminary mechanical activation of initial individual or mixtures of hydroxides, oxides, metal salts with subsequent hydrochemical treatment in aqueous media (or lack of it), drying, heat treatment, which reduces the temperature of formation of the final products and produces dispersed materials with the given properties, as compared to the traditional method of high-temperature sintering of the same components of mixtures, which requires significantly higher temperatures and synthesis time. For instance, works [27, 28] study in detail the processes of "aging" of mechanically activated gibbsite in aqueous solutions of nitric acid salts $M^{2+}(NO_3)_2$ (where M^{2+} = Zn, Cu, Ni, Co) at room temperature and under autoclave treatment conditions. It is shown that the "aging" of the starting gibbsite (not activated) at room temperature does not provide the formation of complex aluminium compounds with the respective cation. The formation of layered double hydroxides (LDH) is observed only when mechanochemically activated gibbsite products are used under hydrothermal conditions at 150°C for 48 hours. However, it is worth noting that this method has not been widely used due to the lack of appropriate industrial equipment.

In addition to mechanochemical activation of GB, among the known methods that have received the widest practical application in the production of carriers, catalysts, and desiccants, methods of rapid heating of gibbsite powder carried out in various apparatuses, so-called “flash” processes [30–32], were obtained. We highlight two of them, viz. a method of thermochemical activation (TCA) [30] and centrifugal thermal activation (CTA) developed in the Institute of Catalysis of the Siberian Branch of the Russian Academy of Sciences [32]. Gibbsite thermal activation products (CTA-GB and TCA-GB), as compared to the initial GB, are characterized by increased chemical activity with respect to electrolytes, viz. higher dissolution rates in acids and alkalis [32]. Due to these properties, the products of rapid heating of the GB powder, including by the CTA method, can be promising for the production of complex ACO systems with different Co_3O_4/Al_2O_3 ratios, including spinel structures such as $CoAl_2O_4$ and Co_2AlO_4. Thus, one can expect the increased reactivity of CTA-GB products upon contact with aqueous solutions of cobalt salts, which will provide Co-aluminum materials with the given elemental composition under mild conditions without the classic stages of co-precipitation (sol-gel technology), high temperature sintering, and mechanochemical activation.

Earlier, in [33–36], we showed the fundamental possibility of using the product of centrifugal thermal activation of gibbsite (CTA-GB) to obtain Mg-, Ni, Ba, and Cu-aluminum systems of stoichiometric composition $MeAl_2O_4$ (where Me = Mg^{2+}, Ba^{2+}, Ni^{2+}, and Cu^{2+}) by hydrochemical treatment of thermal activation products CTA-GB in solutions of magnesium nitrate, barium, nickel, as well as copper

under hydrothermal and "soft" conditions (at room temperature). As compared to the traditional ceramic method, this reduces the calcination temperature mode and produces a highly dispersed product (magnesium or barium aluminate), and, when compared with the classical co-precipitation method, allows to significantly reduce the amount of initial reagents, process stages, as well as to minimize or completely eliminate the formation of wastewater and harmful nitrogen oxides (NO_x) in waste gases at heat treatment stages in cases of partial washing of precipitates from occluded impurities. This makes this method very attractive for various applications, including the preparation of supports and catalysts with reduced surface acidity, which is of great importance in preparing catalytic systems for hydrocarbon dehydrogenation/hydrogenation processes, developing new materials and improving existing ones, including in the field of hydrogen energy.

The purpose of this work is to synthesize and study high-percentage alumina-cobalt oxide systems formed during hydrochemical/hydrothermal treatment of products of centrifugal thermal activation of gibbsite in cobalt nitrate solutions and subsequent heat treatment of formed xerogels at temperatures in the range 350–850°C.

EXPERIMENTAL PART

As an initial raw material for obtaining the product of centrifugal thermal activation of gibbsite (CTA-GB) of IK-02-76 grade (TU 2175-040-03533913-2007), we used gibbsite (G) produced by Achinsk Alumina Plant of GD 000 grade (TU-1711-99-039-2000). The content of impurities in the initial gibbsite (in wt%) was Fe = 0.002, Na = 0.11, K = 0.033, and Si = 0.014. The value of the specific surface area of the initial gibbsite powder was not more than 1 m^2/g. The loss on calcination at 850°C was 34 wt%. Cobaltous nitrate hexahydrate $Co(NO_3)_2 \cdot 6H_2O$ (puriss. p.a., VECTON) was used as the initial Co-containing raw material. Gibbsite (γ-$Al(OH)_3$) has a hexagonal crystal structure, which is based on a double layer AB of densely packed hydroxyl groups (OH-groups). At the same time, two thirds of the octahedral vacancies are filled with Al^{3+} cations, each of which is octahedrally surrounded by six OH-groups. Combining the GB double layers into packages can be depicted by the sequence ABBAABBA, etc. The double layers are held together by hydrogen bonds (H-bonds), with the distance between two neighboring layers A or B being 2.81 Å as compared to 2.03 Å, the distance between layers A and B [37, 38].

The thermal activation of gibbsite was carried out in a drum-type centrifugal flash reactor (CEFLAR^{TM}) at the temperature of thermoelectric heaters 540 ± 5°C, a drum rotation speed of 60 rpm, and a flow rate of the initial powder of 40 kg/h. The CTA-GB product was further subjected to grinding in a ball mill for 6h, which provided a powder with an average particle size of about 30–40 microns. The loss on calcination of the obtained CTA-GB product at 850°C (4 h) was about 12–13 wt%.

To synthesize ACO samples, CTA-GB was loaded into the previously prepared cobalt nitrate solution so that the cation ratio corresponded to stoichiometric cobalt aluminate ($CoAl_2O_4$). The suspension with an initial pH value of about 4.5 was hydrothermally treated at 150°C for 4 h with stirring at 120–150 rpm, or incubated under "mild" conditions at room temperature and also under hydrothermal conditions at 150°C for 4 h. The gels formed by hydrochemical/hydrothermal treatment without a preliminary washing step were dried at 110°C for 6 h to a xerogel state. Subsequent heat treatment was carried out in a muffle furnace in air at temperatures of 350–850°C for 4 h. Samples are designated as Co-Al(T_1)-T_2 in the text, where T_1 is the hydrochemical/hydrothermal treatment (hydration) temperature of the suspensions (°C), and T_2 is the final sample treatment temperature (°C). The names of the samples used in the work are transcribed below in Table 1.

Total cobalt content in the samples was analyzed by atomic emission spectroscopy with inductively coupled plasma on OPTIMA 4300 DV (PERKIN ELMER).

The X-ray phase analysis was performed with an ARL-X'TRA diffractometer using CuK_α (λ = 1.5418 Å). The samples were scanned with a step of 0.05° in the region of angle values 2θ = 10–70° and accumulation time of 3 s. Identification of phases was carried out by comparing experimental diffractograms with diffractograms in the PDF 2 database.

Thermal analysis of the samples was carried out on a STA 449C Jupiter synchronous thermal analysis unit (NETZSCH). Alumina crucibles were used to examine the samples. The air supply rate to the sample chamber was 30 ml/min; the inert gas (argon) was supplied to the weighing unit at a rate of 20 ml/min. The samples were heated at a rate of 2°C/min from room temperature to 50°C and held at this temperature for 30 minutes. Then, temperature-programmed heating to 1000°C at a rate of 10°C/min was carried out.

Texture characteristics were obtained by low-temperature nitrogen desorption at 77 K on an automated Quadrasorb-EVO Quantachrome (USA) unit. The samples were studied in the form of powders with their

Table 1. Names of samples, their interpretation and brief synthesis methodology.

Sample name	Detailed interpretation	Brief preparation method
GB	crystalline gibbsite (aluminum hydroxide γ-$Al(OH_3)$)	gibbsite produced by Achinsk Alumina Refinery, grade GD 000 (TU-1711-99-039-2000)
CTA-GB	product of centrifugal thermal activation of crystalline gibbsite	prepared by thermoactivation of gibbsite in a drum-type centrifugal flash reactor (CEFLARTM) at 540 ± 5°C
B	well oxidized aluminum hydroxide boehmite – γ-AlOOH	synthesized by hydrothermal treatment of gibbsite in saturated water vapor at 250°C for 4–6 h. The paste was dried at 110°C for 6 h to constant weight
PB	aluminum hydroxide pseudoboehmite – γ-$AlOOH{\cdot}xH_2O$	was synthesized by simultaneous pouring of equinormal aqueous solutions of $Al(NO_3)_3{\cdot}9H_2O$ salt and ammonium hydrogen carbonate at constant pH 7.0. The mixed solutions were incubated at 80°C for 4 h to obtain pseudoboehmite precipitate. The resulting precipitate was separated from the aqueous solution by decantation, washed of impurities with distilled water, and dried in the air flow at 110°C for 6 h to constant weight
BA	well oxidized aluminum hydroxide bayerite – α-$Al(OH)_3$	prepared by precipitation of Al^{3+} ions from the aqueous solution of $Al(NO_3)_3{\cdot}9H_2O$ salt. The suspension was kept at pH 10.0 and 90°C for 12 h. After that, the obtained gel was washed from impurities and dried to constant weight at 110°C to obtain xerogel
CoAl-COG-110	comparison sample of alumina-cobalt system obtained by classical co-precipitation method	prepared by the classical method of Al^{3+} and Co^{2+} co-precipitation from mixed aqueous solutions of $Al(NO_3)_3{\cdot}9H_2O$ and $Co(NO_3)_2{\cdot}6H_2O$ salts under the following conditions: co-precipitation pH 9.0–9.5, cation ratio in the initial mixed aqueous solution Al/Co = 2)
CoAl-COG-550	heat treatment product of CoAl-COG-110	obtained by calcination of CoAl-CP-110 in air at a final temperature of 550°C for 4 h
Al(150)-110	product of hydration (interaction) of CTA-GB with water dried at 110°C	prepared by hydration (interaction) under conditions of hydrothermal treatment at 150°C for 4 h of activated CTA-GB in water (without Co^{2+} cations). The formed gel was dried at 110°C for 6 h to constant weight
CoAl(25)-110	dried product of hydration (interaction) at room temperature of CTA-GB with aqueous solution of nitrate-nitrate Co^{2+}	prepared under room treatment conditions for 4 h of activated CTA-GB and $Co(NO_3)_2{\cdot}6H_2O$. The formed gel without stages and washing and decantation was dried at 110°C for 6 h to constant weight
CoAl(150)-110	hydration product (interaction) under hydrothermal treatment at 150°C of activated CTA-GB with aqueous solution of nitrate Co^{2+}	prepared under conditions of hydrothermal treatment at 150°C for 4 h of activated CTA-GB and $Co(NO_3)_2{\cdot}6H_2O$. The formed gel without stages and washing and decantation was dried at 110°C for 6 h to constant weight
CoAl(25)-550	CoAl(25)-110 heat treatment product	prepared by heat treatment in air for 4 h at 550°C
CoAl(25)-850	CoAl(25)-110 heat treatment product	prepared by heat treatment in air for 4 h at 850°C
CoAl(150)-550	CoAl(150)-110 heat treatment product	prepared by heat treatment in air for 4 h at 550°C
CoAl(150)-850	heat treatment product CoAl(150)-110	prepared by heat treatment in air for 4 h at 850°C

preliminary vacuum treatment at 300°C for 2 h. The methods of measurement and calculation of textural parameters complied with ASTM D3663, ASTM D4820, ASTM D1993, UOP425-86.

Temperature-programmed hydrogen reduction (TPR-H_2) of the samples was carried out on a Khemosorb unit (Neosib, Russia). Before reduction, the samples (50 mg, 0.25–0.5 mm fraction) were heated for 1 h in the Ar atmosphere at 200°C. The reduction was carried out at a heating rate of 10 deg/min in the H_2/Ar flow with a concentration of 9.7 vol.%. The absorption of H_2 was determined using a thermal conductivity detector. The resulting water was condensed at –60°C before the gas was introduced into the detector.

The morphology of the calcined samples was examined using a JSM-6460 LV scanning electron microscope (JEOL) with a probe electron energy of 20–25 keV. The microscope was equipped with an INCA Energy-350 X-ray energy dispersive spectrometer (Oxford Instruments).

DISCUSSION OF RESULTS

Previously, it was shown by the X-ray phase analysis that the initial gibbsite used for thermal activation is well oxidized [34, 36], with no other phase impurities of inclusions detected in it. As a result of thermal activation, the diffractogram of CTA-GB shows a blurred "halo" in the region of angles $2\theta = 20–40°$, indicating the presence of X-ray amorphous alumina, reflections from crystalline boehmite (γ-AlOOH) formed in the process of centrifugal thermal activation in massive 3D-monocrystals of gibbsite of micron sizes, and also peaks of initial undecomposed gibbsite [23].

One knows that during synthesis of complex Co-aluminum materials by different variants of sol-gel technology (co-precipitation techniques), depending on the conditions, it is possible to form, in addition to the main precipitate, such aluminum hydroxides as pseudoboehmite, boehmite, bayerite, and combinations of their mixtures [25, 30–32]. In this regard, for further interpretation of physicochemical data for the synthesized Co-aluminum systems based on CTA-GB in this work, samples of comparison of individual aluminum hydroxides of pseudoboehmite, boehmite, and bayerite were prepared according to the classical synthesis schemes (Table 1), the X-ray phase analysis data of which are shown in Fig. 1. We give some structural features of these hydroxides. The crystal structure of bayerite (α-$Al(OH)_3$) is similar to that of GB and is a hexagonal densely packed structure of double layers of OH-groups with $^2/_3$ octahedral voids filled with Al^{3+} cations. The double layers are connected to each other in packets in the ABABAB sequence and are held together by H-bonds. Within a double layer, the AB distance is 2.07 Å and the distance between two double layers is 2.64 Å. Due to this combination of double layers, the minimum O – O distance between two neighboring layers is larger in BA (3.13 Å) than in GB (2.81 Å) [38].

In boehmite (γ-AlO(OH)), aluminum atoms are surrounded by a deformed octahedral grouping of oxygen atoms. These octahedra join together to form a complex layered structure [39]. When discussing issues related to boehmite, a clear distinction should be made between well-oxygenated BE and pseudoboehmite (γ-AlO(OH) × nH_2O) (microcrystalline boehmite). Thus, pseudoboehmite is understood as a poorly oxidized aluminum compound of the composition $Al_2O_3 \cdot xH_2O$ ($2.0 > x > 1.0$) with interplanar distances increased in the 020 direction to 6.7 Å as compared to 6.12 Å for boehmite [40]. One knows that pseudoboehmite differs from boehmite by the presence of additional (as compared to the structural formula) water molecules located in the interlayer space and having a loosening effect on the structure [38, 41].

The X-ray phase analysis data show that the comparison sample (Fig. 1a) is a PB and contains traces of impurity phase of bayerite, which takes place with this method of preparation [29, 32, 42]. The comparison samples of boehmite and bayerite are well crystallized systems without any additional phase inclusions (Fig. 1b). The comparison sample Al(150)–110 was obtained by hydration (interaction) under conditions of hydrothermal treatment at 150°C for 4 h of activated CTA-GB in water (without Co^{2+} cations), reflecting the phase state of the hydrated system without cobalt, and, by phase composition, is aluminum hydroxide with the structure of pseudoboehmite, PB (Fig. 1c). Note that as a result of heat treatment of the considered individual aluminum hydroxides in the temperature range of 450–650°C [32, 42], individual or mixed low-temperature modifications of aluminum oxides γ-Al_2O_3 and/or η-Al_2O_3 are formed (Fig. 1d).

The diffraction pattern of the dried CoAl-COG-110 product synthesized by the classical co-precipitation method indicates the presence of only the LDH compound with impurities of the bayerite phase (Fig. 2a). The formation of the bayerite phase is due to the fact that the CoAl-COG-110 system was formed in an alkaline environment, which is favorable for forming this hydroxide modification (Fig. 1c, *2*) [25, 32, 36]. After heat treatment of CoAl-COG-110 at 550°C, the diffractogram of the calcination product

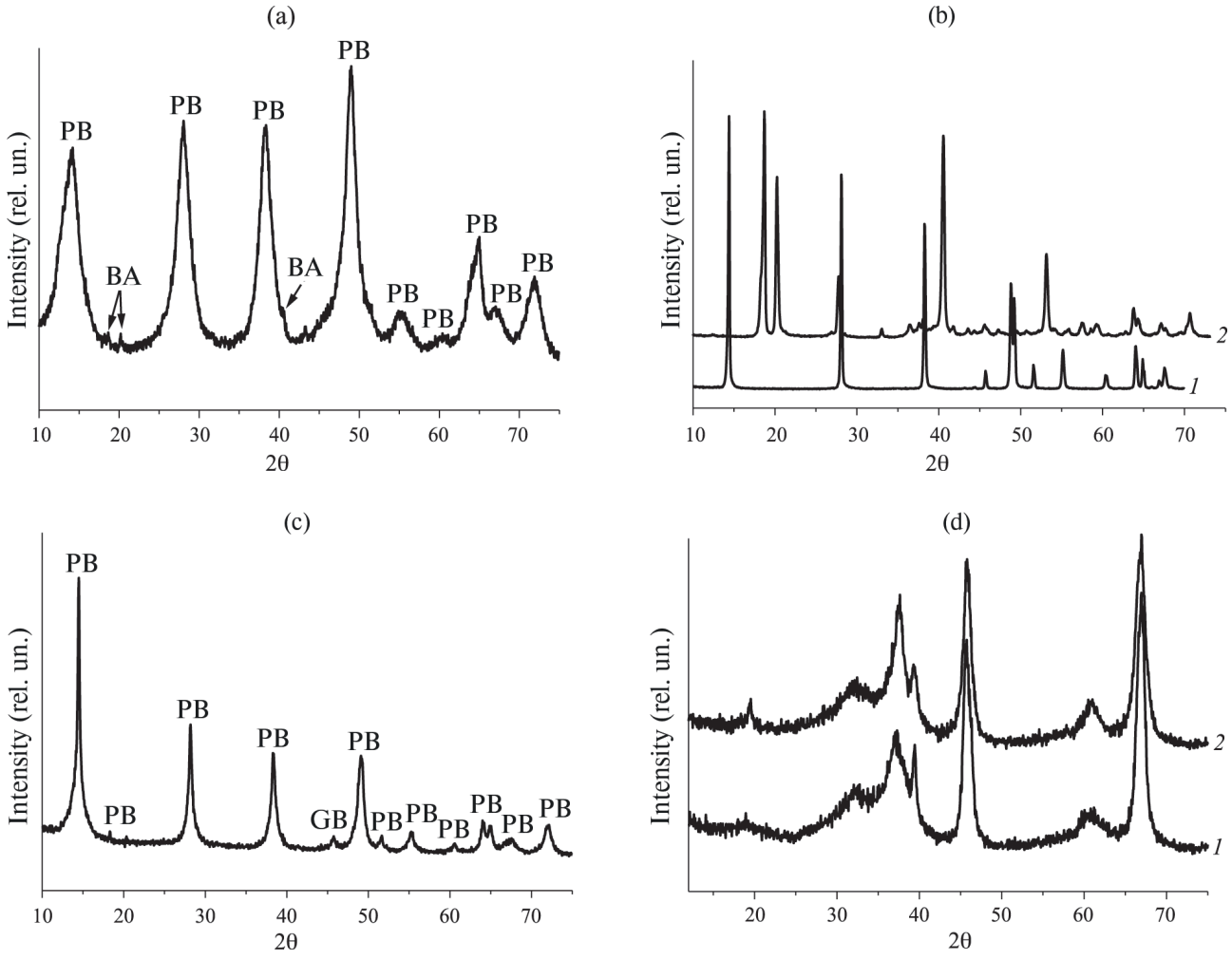

Fig. 1. Powder diffractograms of comparison samples of aluminum hydroxides and oxides — (a) pseudoboehmite synthesized by the classical nitrate precipitation method, (b) well-oxidized boehmite (*1*), well-oxidized bayerite (*2*), (c) Al(150)-110 hydration product of CTA-GB in the aqueous medium (without presence of Co^{2+} cations), representing pseudoboehmite, and (d) products of heat treatment at 550°C of boehmite/pseudoboehmite and bayerite that are low-temperature modifications of γ-Al_2O_3 (1) and η-Al_2O_3 (2), respectively.

CoAl-COG-550 (Fig. 2b) shows diffraction lines, which are equally likely to belong to spinels of Co_3O_4 and/or $CoAl_2O_4$ type, as well as their mixtures. At the same time, it is important to note that publications show that when analyzing alumina-cobalt spinel materials obtained by different methods (co-precipitation, deposition, high-temperature sintering of mechanical mixtures, etc.) by X-ray phase analysis method, the observed positions of diffraction peaks can equally likely indicate a compound of Co_3O_4, $CoAl_2O_4$, as well as their mixed combinations due to the proximity of the positions of diffraction maxima of these compounds [2, 5, 23]. In this case, other physicochemical methods of analysis are effective for detailed interpretation and identification, which will be further considered and shown in the work while discussing the results.

According to X-ray phase analysis data, in samples of hydrothermal interaction of CTA-GB in aqueous solutions of Co^{2+} nitrate in the concentration range of 10–33 wt% (Figs. 2c and 2d), a significant difference is recorded as compared to CoAl-COG-110 (Fig. 2a). The first thing to note is that at cobalt contents below the stoichiometric cobalt content in the cobalt concentration range of 10–20 wt% by X-ray phase analysis, the PB phases as well as the phase of the initial cobalt nitrate salt are reliably detected in the samples (Fig. 2c). Secondly, when the cobalt concentration is increased to the stoichiometric content (~33 wt%), the formation of pseudoboehmite is not detected by the X-ray phase analysis, and the observed phase is cobaltous nitrate (Fig. 2d). The latter is in good agreement with the thermal analysis data of the same samples presented below. Note that bayerite is not formed, as compared

to the co-precipitated CoAl-COG-110 comparison system, because synthesis was performed in weakly acidic (acidic) aqueous suspensions, which are not favorable media for bayerite.

In addition, the X-ray phase analysis method did not reveal any qualitative and quantitative distinctive features in the phase composition of alumina-cobalt compositions when varying such synthesis parameters as cobalt concentration, hydrochemical synthesis temperature, and final temperature treatment in the range of 350–850°C (Fig. 2e). At the same time, the observed positions of the diffraction peaks can equally likely indicate compounds of both Co_3O_4 and $CoAl_2O_4$ types, as well as their mixed combinations, due to the proximity of the positions of the diffraction maxima of these spinels as shown above, which is equivalent to the case of the classically prepared alumina-cobalt spinel CoAl-COG-550 (Fig. 2b). Note that the X-ray phase analysis method failed to find individual phases of aluminum oxides in calcined systems at 350–850°C as well as in the comparison sample CoAl-CP-550 were not detected.

The analysis of thermal analysis data yields that the initial gibbsite is characterized by a total weight loss of ~34 wt% and the presence of the following endothermic effects, viz. endo-effect at 97°C caused by the removal of weakly bound molecular water; the double pre-effect with maximums at 238 and 256°C, indicating the initial stage of decomposition of crystallites of the lamellar form of gibbsite with the formation of boehmite; the endothermic effect of dehydration of the gibbsite phase (peak at 314°C) and endo-effect of decomposition of the boehmite phase at 536°C [32, 36].

The heating curve of the product of centrifugal thermal activation of gibbsite CTA-GB (Fig. 3a) shows the endothermic effect with the minimum at 124°C due to the removal of molecular water from the X-ray amorphous alumina component of the thermal activation product. The endo effect with minimum at 257°C due to dehydration of residual gibbsite phase and endothermic thermal effect with minimum at 483°C due to decomposition of residual boehmite contained in CTA-GB are preserved. The presence of the exothermic thermal effect with the maximum at 832°C indicates the crystallization of the X-ray amorphous phase into low-temperature forms of Al_2O_3 [30–32]. Note that the appearance of exothermic thermal effects with maximums at 800–850°C in gibbsite products thermally activated by rapid heating methods, including those obtained by centrifugal thermal activation, indicates the crystallization of the X-ray amorphous phase into the low-temperature form of γ- Al_2O_3 or η- Al_2O_3 [30, 32]. The appearance of endothermic thermal effects with minimums at 450–500°C on the heating curve in the comparison sample Al(150)-110 (Fig. 3b), which is a product of CTA-GB crystallization in aqueous medium (without Co^{2+} cations), indeed indicates that the system is pseudoboehmite, which is also, as shown above, in good agreement with the X-ray phase analysis method (Fig. 1c).

From the results of studying thermal analysis data, significant differences were found, as compared to the original CTA-GB and Al(150)-110, in the products of hydrochemical treatment of CTA-GB in Co^{2+} solutions (with cobalt concentrations of 10, 15, 20, and 33 wt%) dried at 110°C (Fig. 3). When CTA-GB interacted with aqueous solutions of cobalt nitrate with cobalt content of 10–20 wt% (below stoichiometric. % (below the stoichiometric content), transformations in the Co-CTA-GB system proceed in the direction of pseudoboehmite formation, which is evident from the presence of endo-effects at 450–460°C on the thermograms of hydrothermal samples 10CoAl(150)-110, 15CoAl(150)-110, and 20CoAl(150)-110 (Figs. 3c and 3d), which agrees with the X-ray phase analysis data of the samples (Fig. 2c, *1–3*). Moreover, the appearance of endothermic thermal effects with minimums at 210–270°C indicates the thermal decomposition of alumina-cobalt layered double hydroxides (LDH-hydrotalcites, which are compounds with a layered-grid structure) formed at the synthesis stages, for which, as one knows from publications, the specified temperature range is a sign of their presence [1, 25]. The presence of endothermic peaks at 305–365°C is due to the decomposition of the initial cobalt nitrite (Figs. 3c and 3d), which is also detected by the X-ray phase analysis (Fig. 2c).

With the increase of Co^{2+} concentration up to its stoichiometric value (33 wt%), both at room temperature (sample 33CoAl(25)-110) and under hydrothermal conditions (sample 33CoAl(150)-110), aluminum hydroxide phases with pseudoboehmite structures are not formed, which is evident from the absence of endothermic thermal effects (450–460°C) characteristic of boehmite on thermograms of interaction products (Figs. 2f and 2g). We found similar changes earlier when studying the interaction of CTA-GB products with aqueous solutions of nickel nitrate salts [35]. Thus, comparing the data of this work and the results in [35], we can testify that, other conditions of interaction being equal and in the case of stoichiometric ratio of cobalt or nickel to aluminum (one mole of Co^{2+} or Ni^{2+} per two moles of Al^{3+}), pseudoboehmites in Co-CTA-GB and Ni-CTA-GB systems are not formed.

As it was shown above by X-ray phase analysis method, it is difficult to distinguish Co_3O_4 or $CoAl_2O_4$

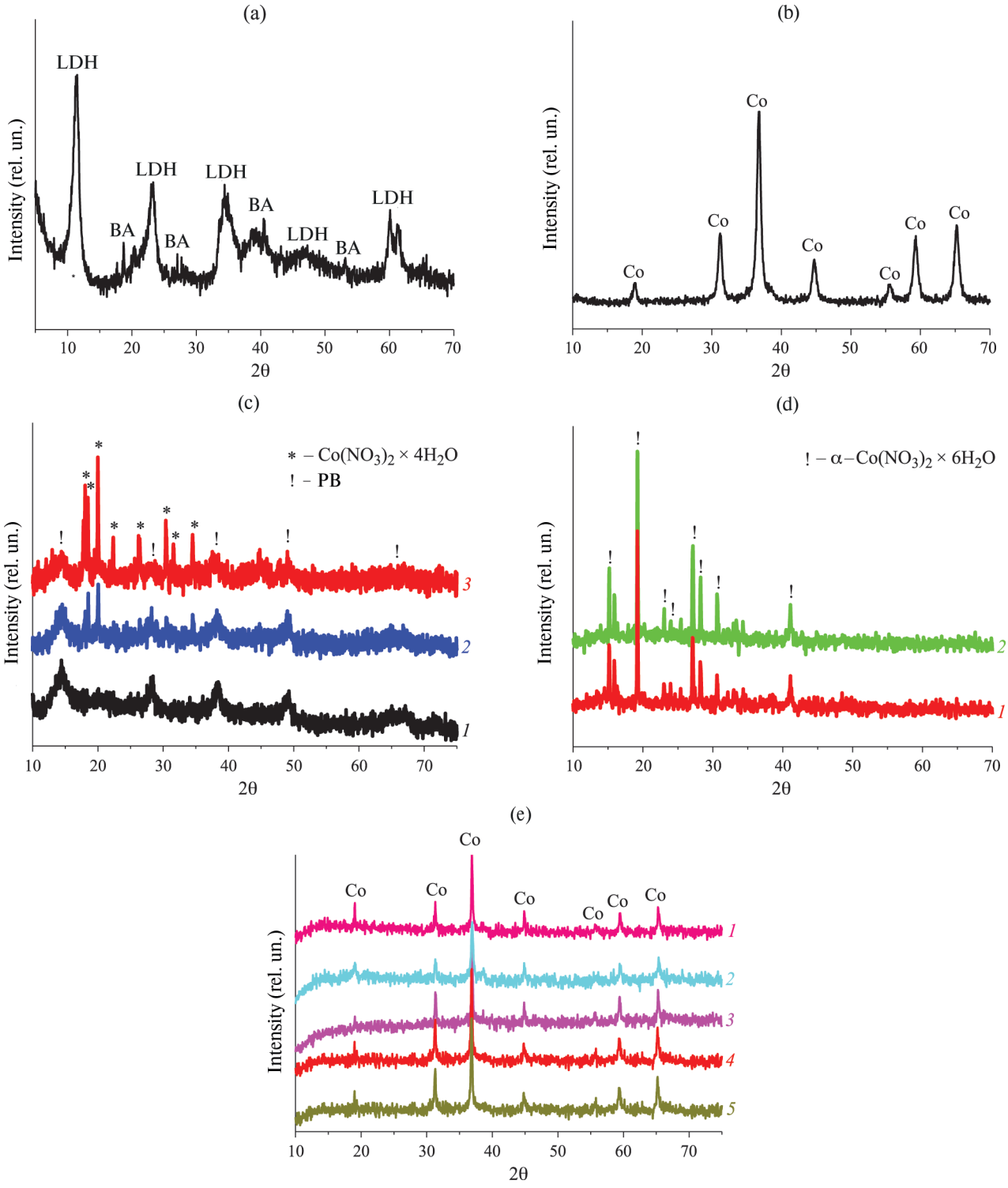

Fig. 2. Powder diffractograms of alumina-cobalt systems after low-temperature drying at 110°C and heat treatment in the range of 350–850°C — (a) comparison sample CoAl-COG-110 synthesized by the conventional co-precipitation method using nitrate technology, (b) comparison sample CoAl-COG-550 prepared by heat treatment of CoAl-COG-110 at 550°C, (c) products of hydrothermal treatment of CTA-GB in Co^{2+} solutions in the concentration range of 10–20 wt%: (*1*) 10CoAl(150)-110, (*2*) 15CoAl(150)-110, (*3*) 20CoAl(150)-110, (d) products of room and hydrothermal treatment of CTA-GB in Co^{2+} solutions with stoichiometric concentration of ~33 wt%: (*1*) 33CoAl(150)-110, (*2*) 33CoAl(25)-110, (e) products of heat treatment of samples in the range 350–850°C of hydrochemical interaction of CTA-GB in Co^{2+} solutions with stoichiometric concentration of ~33 wt%.: (*1*) CoAl(25)-350, (*2*) CoAl(25)-550, (*3*) CoAl(25)-850, (*4*) CoAl(150)-550, (*5*) CoAl(150)-850.

phases with the spinel structure, therefore to understand if one or another phase is present and estimate their content, we performed the research by the TPR-H_2 method. Figure 4 shows the temperature-programmed hydrogen reduction curves of the CoAl(25)-350, CoAl(25)-550, CoAl(150)-550, CoAl(25)-850, and CoAl(150)-850 samples containing stoichiometric amount of cobalt (33 wt%). Table 2 summarizes the recovery characteristics of the samples such as the total hydrogen absorption, the amount of hydrogen absorbed in individual peaks, as well as the temperature maxima of hydrogen absorption and the calculated percentage of Co_3O_4/$CoAl_2O_4$ type spinels in the samples. One knows from publications that for individual Co_3O_4 oxides there is a stepwise reduction of $Co^{3+}\rightarrow Co^{2+}\rightarrow Co^0$, which, as a rule, is evidenced on the TPR-H_2 curves by two temperature reduction regions 180-270 °C and 270-up to 500°C [12, 43, 44]. In mixed systems of cobalt with aluminum, in alumina-cobalt spinels, the temperature regions of the reduction of cobalt, more firmly bound to aluminum, begin above 500°C and continue up to 700–800°C [12].

The obtained TPR-H_2 data show that for all studied samples two temperature regions of reduction are observed, the first of which is characterized by the absorption maximum at 330–350°C, due to the reduction of cobalt in Co_3O_4 phases to Co°, the second is in the range from 510 to 800°C associated with the process of reduction of cobalt Co^{2+} in the spinel $CoAl_2O_4$ to Co° (Fig. 4, Table 2). The data also show that the maximum amount of hydrogen absorbed is in the Co-Al(25)-350 sample (Fig. 4a) calcined at the lowest temperature of 350°C. At the same time, for the same Co-Al(25)-550 sample (Fig. 4b), the total amount of absorbed hydrogen is markedly reduced as a result of higher calcination temperature, which provides a greater depth of interaction between cobalt oxide and aluminum oxide. At the same time, comparison of TPR-H_2 data for Co-Al(25)-550 (Fig. 4b) and CoAl(150)-550 (Fig. 4c) obtained under hydrochemical and hydrothermal treatment conditions, respectively, and calcined at the same temperature, shows that deeper interaction in the Co-CTA-GB system is provided by hydrothermal synthesis.

The samples CoAl(25)-850 and CoAl(150)-850 subjected to higher heat treatment at 850°C are almost completely transformed into the $CoAl_2O_4$ spinel (Table 2). Thus, the sample CoAl(150)-850 contains about 10% of the Co_3O_4 phase (the rest is the spinel $CoAl_2O_4$), and CoAl(25)-850 contains about twice (22%) more Co_3O_4 (the rest is the spinel of $CoAl_2O_4$ type). Thus, the presented TPR-H_2 data show that reduction of cobalt cations in the prepared oxide systems is influenced not only by the final temperature of heat treatment of samples, which is known from publications, but also by the treatment mode of suspensions at the stages of hydrochemical/hydrothermal interaction. At that, hydrothermal conditions are more favorable for spinels of $CoAl_2O_4$ type to be formed.

Below, Table 3 combines the qualitative and quantitative results on phase composition according to X-ray phase analysis and TPR-H_2 for alumina-cobalt samples in the initial dried state (before heat treatment) after room and hydrothermal interaction in the presence of Co^{2+} solutions followed by low-temperature drying and heat treatment at 350–850°C.

We consider the nitrogen porosimetry data presented in Fig. 5 and generalized in Table 4 on the example of systems 33CoAl(25) and 33CoAl(150), reflecting the influence of such synthesis parameters as room/autoclave treatment conditions and varying the temperature of calcination of these systems in the range of 350–850°C. We can see that in the temperature treatment range of 350–550°C, the maximum of the values of specific surface areas is reached for the temperature of 350°C, both for the room synthesis sample and for the sample after hydrothermal treatment. At the same time, the average pore diameter is approximately the same (3.8 nm) and the maximum pore volume (0.20 cm^3/g) is detected for the 33CoAl(150)-550 sample obtained under hydrothermal conditions. Noticeable changes in the textural characteristics can be seen after temperature treatment at 850°C. Thus, for samples 33CoAl(25)-850 and 33CoAl(150)-850, there is a strong decrease in the values of specific surface area (by about 100 m^2/g). Although the total pore volume is practically independent of the calcination temperature for the samples after hydrochemical treatment and increases for the samples after hydrothermal synthesis the average pore diameter shifts markedly towards larger values for both series (Table 4).

Desorption curves show that the samples are characterized by a wide distribution of pore sizes from 3 to 200 nm (Fig. 5), and nitrogen adsorption/desorption isotherms (data not shown but available) most closely corresponds to the H3 hysteresis form type, according to the IUPAC classification, which implies that the prepared alumina-cobalt oxide systems are characterized by the presence of unclosed pores between particles.

The method of scanning electron microscopy also established distinctive features in morphology at varying conditions of synthesis of cobalt-CTA-GB system, which is demonstrated on the example of stoichiometric

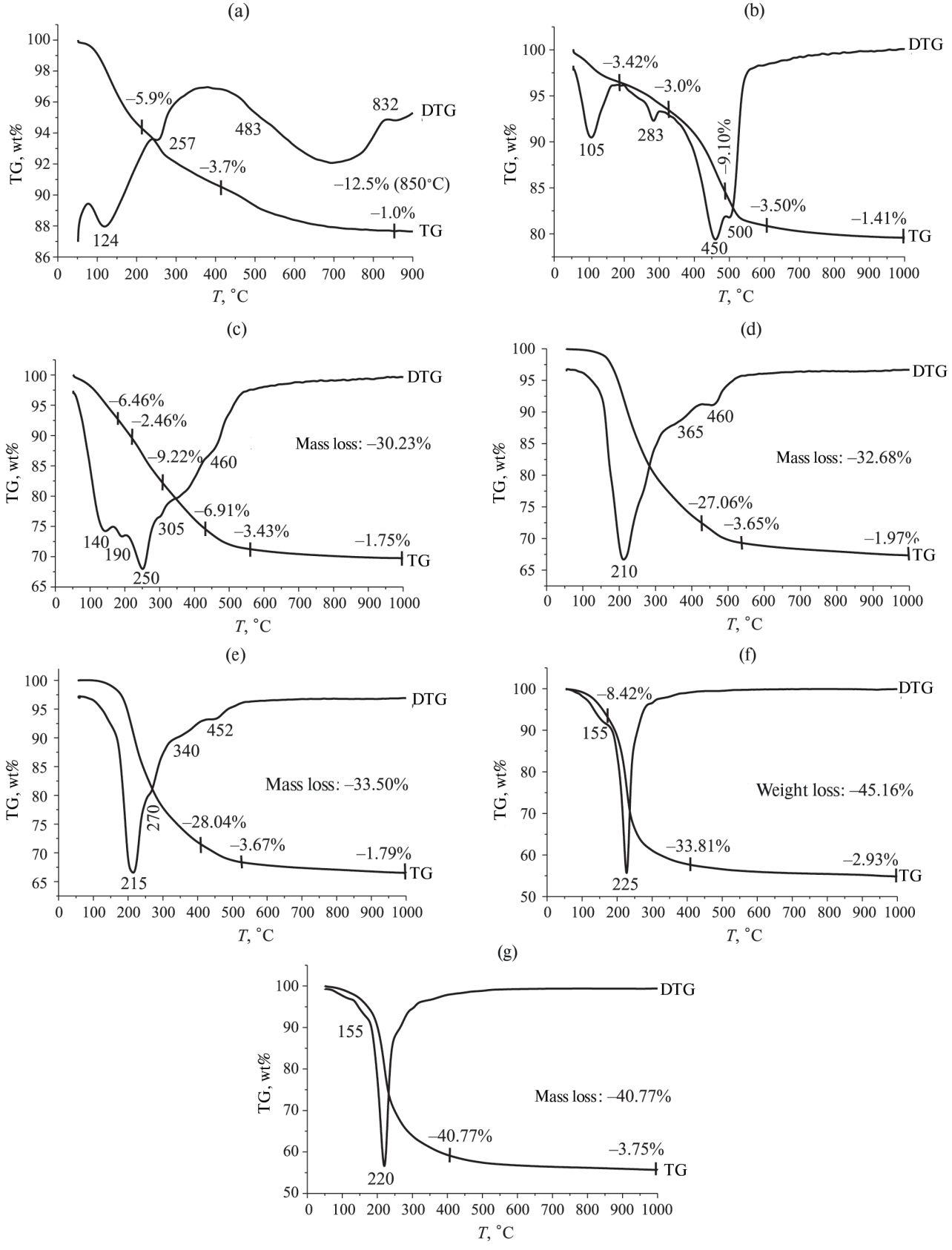

Fig. 3. Thermal analysis data — (a) original CTA-GB, (b) Al(150)-110, (c) 10CoAl(150)-110, (d) 15CoAl(150)-110, (e) 20CoAl(150)-110, (f) 33CoAl(25)-110, and (g) 33CoAl(150)-110.

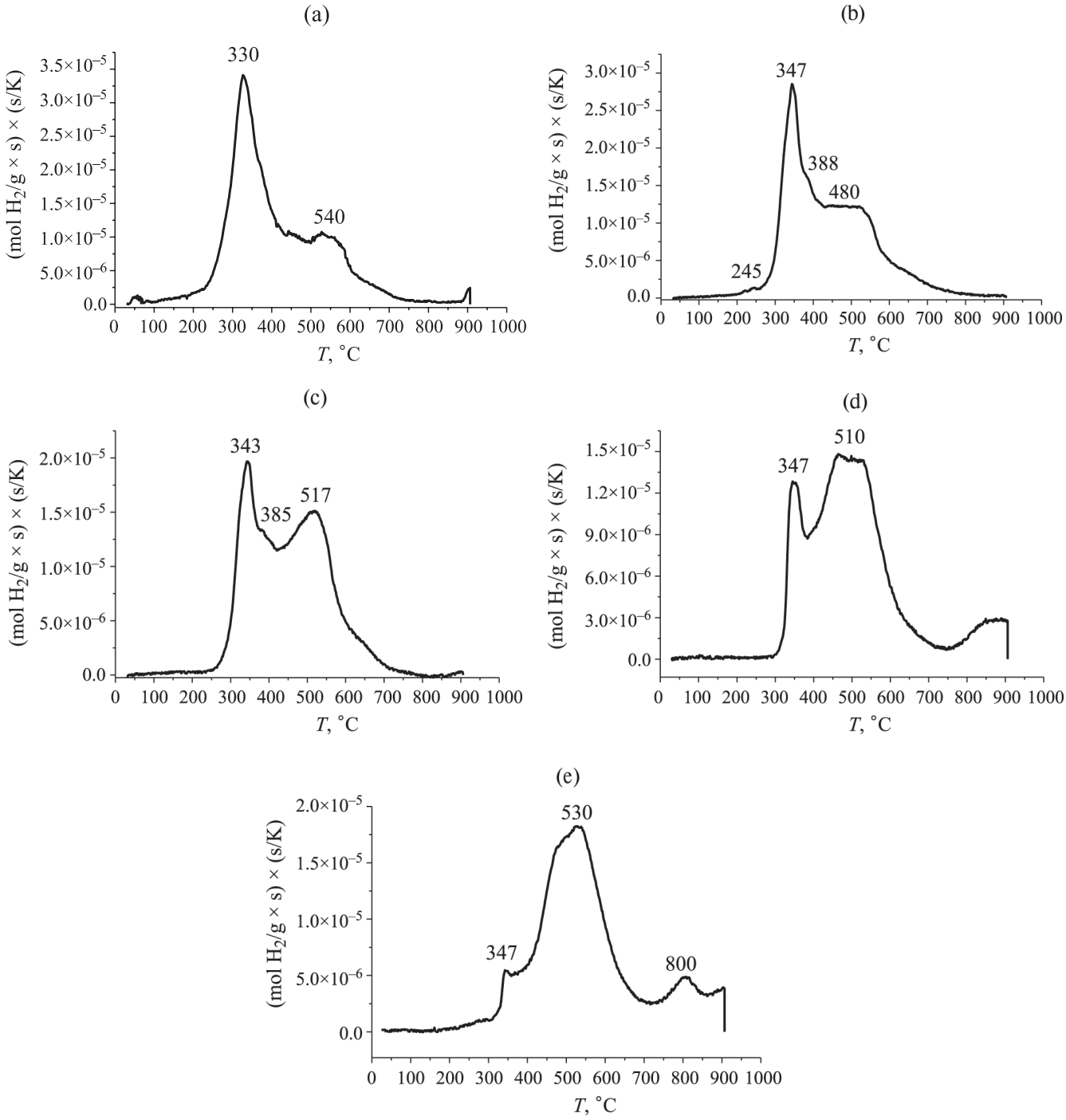

Fig. 4. TPR-H_2 curves — (a) 33CoAl(25)-350, (b) 33CoAl(25)-550, (c) 33CoAl(150)-550, (d) 33CoAl(25)-850, and (e) 33CoAl(150)-850.

samples (with cobalt concentration of 33 wt%) after heat treatment at 850°C.

Thus, according to the data of scanning electron microscopy, the sample 33CoAl(25)-850 and 33CoAl(150)-850 (Fig. 6) consist of faceted 3D-spherical Co_3O_4 and $CoAl_2O_4$ spinel particles, identified above by other physicochemical methods, with sizes in the range of 1–1.5 microns, located on the surface of alumina matrix. Moreover, a larger number of formed 3D spherical particles, apparently Co_3O_4, is objectively observed in the sample 33CoAl(25)-850 as compared to the sample 33CoAl(150)-850 (Fig. 7). Indeed, in the 33CoAl(150)-850 sample, as established above by TPR-H_2 data, the highest hydrogen

Table 2. Recovery characteristics of alumina-cobalt samples according to TPR-H_2 data

Sample	T_{max}, °C	Absorption of H_2 by Co_3O_4, % interval	Absorption of H_2 by $CoAlO_x$, % interval	Quantity of absorbed H_2 per g of the sample $\times 10^{-3}$ mol/g
CoAl(25)-350	330	63	–	3.61
	540	–	37	2.10
				$\sum = 5.71$
CoAl(25)-550	347	45	–	2.15
	480	–	55	2.60
				$\sum = 4.75$
CoAl(150)-550	343	30	–	1.30
	517	–	70	2.94
				$\sum = 4.24$
CoAl(25)-850	347	22	–	0.85
	510–800	–	78	3.0
				$\sum = 3.85$
CoAl(150)-850	347	10	–	0.5
	530–800	–	90	4.0
				$\sum = 4.50$

uptake is in the high-temperature region due to the reduction of cobalt in the $CoAl_2O_4$ structure (Fig. 4d, Table 2).

Using X-ray, thermal, microscopic, and adsorption methods, we studied and showed the possibility of obtaining high-percentage mixed alumina-cobalt spinels with cobalt content (10, 15, 20, and 33 wt%) by hydrochemical treatment at room temperature or under hydrothermal treatment at 150°C of suspensions of the product of centrifugal thermal activation of gibbsite in aqueous solutions of Co^{2+} nitrate with subsequent stages of drying and heat treatment of the formed xerogels.

We showed that heat treatment of hydrothermal interaction products in the range of 350–850°C leads to the formation of mixed oxide systems based on Co_3O_4 and $CoAl_2O_4$spinels characterized by a relatively high specific surface area of 120–150 m^2/g. The ratio between these phases is predominantly determined by such synthesis conditions as the temperature of suspension processing and the final temperature of calcination of the formed xerogels. Hydrochemical treatment of aqueous suspensions of

Table 3. Temperatures and degree of reduction of Co-catalysts

Sample	Sample composition
before heat treatment according to X-ray phase analysis and thermal analysis data	
10CoAl(150)-110 15CoAl(150)-110 20CoAl(150)-110	PB, LDH, cobalt nitrate
33CoAl(25)-110 33CoAl(150)-110	LDH, cobalt nitrate
after heat treatment according to TPR-H_2 data	
33CoAl(25)-350	63% Co_3O_4, 37% $CoAl_2O_4$
33CoAl(25)-550	45% Co_3O_4, 55% $CoAl_2O_4$
33CoAl(25)-850	22% Co_3O_4, 78% $CoAl_2O_4$
33CoAl(150)-550	30% Co_3O_4, 70% $CoAl_2O_4$
33CoAl(150)-850	10% Co_3O_4, 90% $CoAl_2O_4$

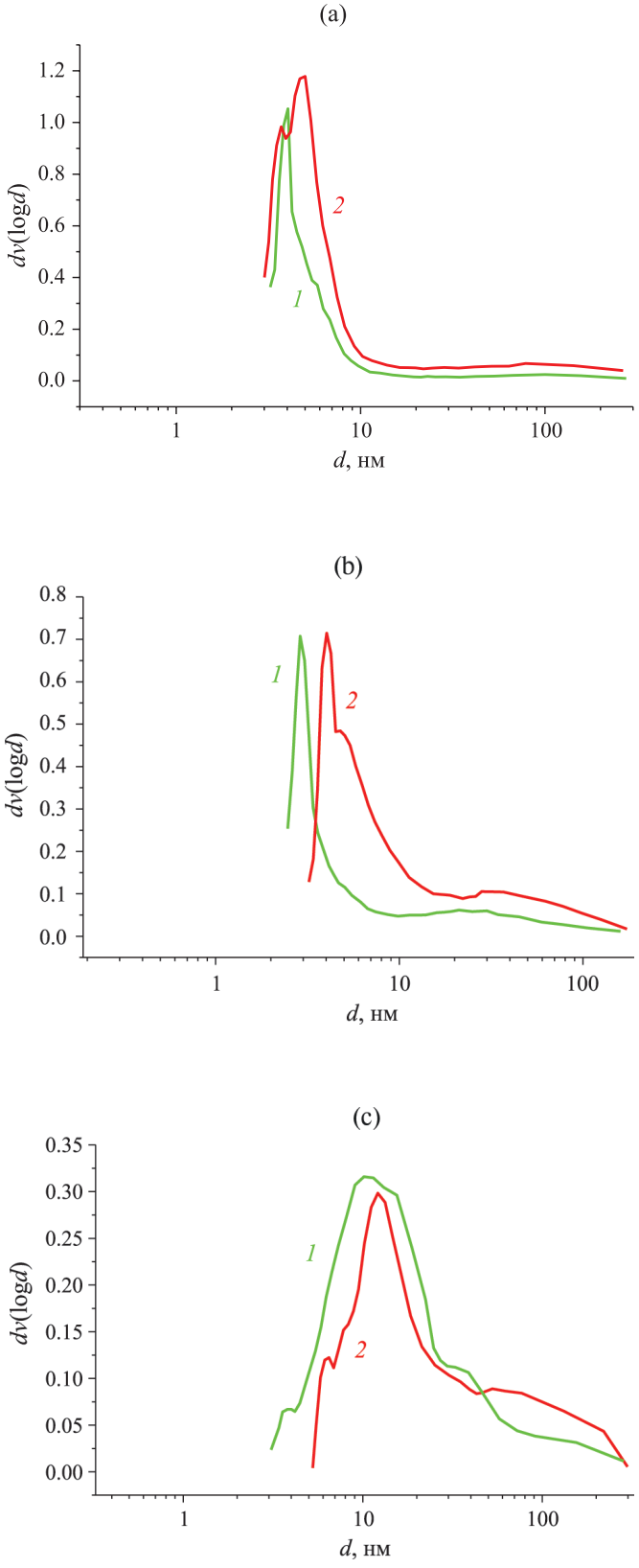

Fig. 5. Desorption curves of pore size distribution — (a) 33CoAl(25)-350 (*1*), 33CoAl(150)-350 (*2*); (b) 33CoAl(25)-550 (*1*), 33CoAl(150)-550 (*2*); (c) 33CoAl(25)-850 (*1*), 33CoAl(150)-850 (*2*).

Table 4. Data of physical nitrogen adsorption for CoAl systems

Sample	S_{sp}, m^2/g BET	V_{por}, cm^3/g (BJH)	D_{por}, nm (BJH)
CoAl(25)-350	128	0.14	3.8
CoAl(25)-550	108	0.11	
CoAl(25)-850	45	0.13	5.2
CoAl(150)-350	155	0.16	3.8
CoAl(150)-550	148	0.20	
CoAl(150)-850	55	0.20	6.8

CTA-GB powder with stoichiometric content of cobalt (~33 wt%) at room temperature provides preferential formation of Co_3O_4 at the calcination temperature of 350°C (~63% according to TPR-H_2 data), while hydrothermal treatment at 150°C leads to deeper interaction of components, which provides formation of predominantly $CoAl_2O_4$ spinels at any temperature modes. Samples after thermal treatment at 850°C are almost completely transformed into the $CoAl_2O_4$ spinel. Thus, after hydrothermal treatment, the system contains about 10% of the Co_3O_4 phase, the rest being the $CoAl_2O_4$ spinel, and after room treatment it contains about twice (22%) more of Co_3O_4, the rest being also the spinel of $CoAl_2O_4$ type.

The obtained results demonstrate a good basis for synthesis of high-percentage alumina-cobalt catalysts based on centrifugal-thermoactivated gibbsite products, including stoichiometric composition, by a low-waste method, reducing the amount of initial reagents, preparation stages, effluents, as well as reducing the total amount of nitrate, as compared to the nitrate classical scheme of co-precipitation of these compounds with similar phase and chemical composition.

ACKNOWLEDGEMENTS

The authors would like to thank Core Facilities VTAN NSU for carrying out the measurements on scientific equipment.

FUNDING

The study was supported by the Russian Science Foundation (grant no. 23-23-00241, https://rscf.ru/project/23-23-00241/).

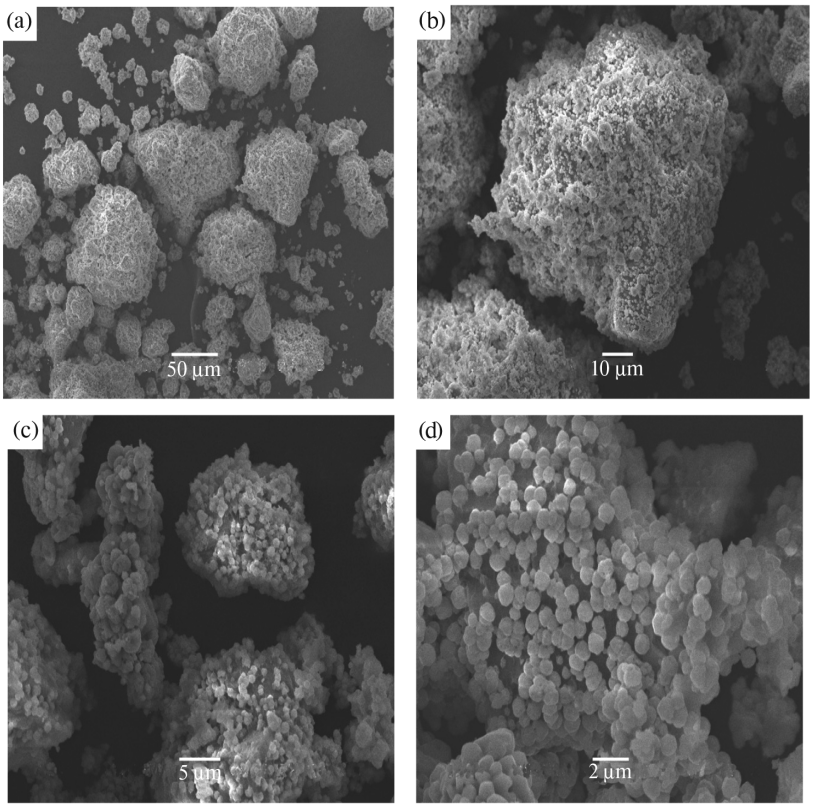

Fig. 6. Electron images of 33CoAl(25)-850 sample particles at different magnifications — 0 (a), 10 (b), 5 (c), and 2 μm (d).

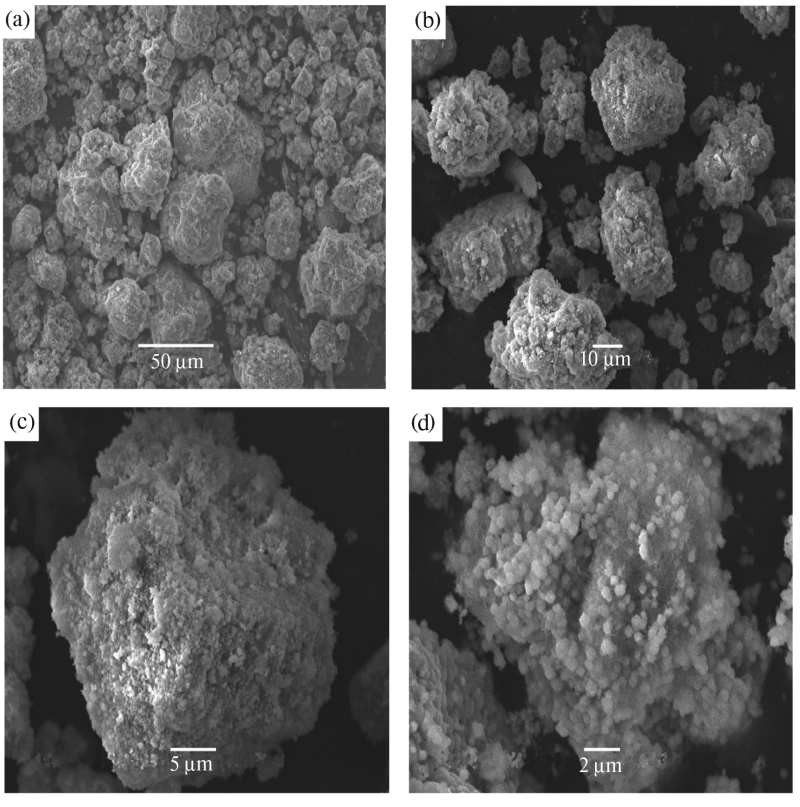

Fig. 7. Electron images of 33CoAl(150)-850 sample particles at different magnifications — 50 (a), 10 (b), 5 (c), and 2 μm (d).

REFERENCES

1. *Li F., Duan X.* // Struct. Bond. 2006. Vol. 119. P. 193.
2. *Tian Li., Huang K., Liu Y. et al.* // J. Solid State. Chem. 2011. Vol. 184. P. 2961.
3. *Merikhi J., Jungk H., Feldmann C.* // J. Mat. Chem. 2002. Vol. 10. P. 1311.
4. *Veronesi P., Leonelli C., Bondioli F.* // Technologies. 2017. Vol. 5. P. 42.
5. *Rangappa D., Ohara S., Naka T. et al.* // J. Mat. Chem. 2007. Vol. 17. P. 4426.
6. *Tang Y., Liu Y., Yu S. et al.* // J. Power Sour. 2014. Vol. 256. P. 160.
7. *Khodakov A.Y., Chu W., Fongarland P. et al.* // Chem. Rev. 2007. Vol. 107. P. 1692.
8. *Jacobs G., Das T.K., Zhang Y. et al.* // App. Catal. A: General. 2002. Vol. 233. P. 263.
9. *Narayanan S., Unnikrishnan R.* // J. Chemical Society, Faraday Transactions. 1998. Vol. 94. P. 1124.
10. *Gandia L.M., Montes M.* // J. Molecular Catal. 1994. Vol. 94. P. 347.
11. *Ragupathi C., Vijaya J.D., Narayanan S. et al.* // Ceram. Intern. 2015. Vol. 41. P. 2069.
12. *Choya A., Rivas B., Gutiérrez-Ortiz J.I. et al.* // Materials. 2019. Vol. 19. P. 1.
13. *Moraz-Lazaro J.P., Blanco O., Rodriguez-Betancourtt V.M. et al.* // Sensor and Actuators B: Chemical. 2016. Vol. 226. P. 518.
14. *Yang He., Goldbach A., Shen W.* // Int. J. Hydrogen Energy. 2024. Vol. 51. P. 1360.
15. *Das T., Kweon S., Nah In. et al.* // Cryogenics. 2015. Vol. 69. P. 36.
16. *Zhuzhgov A.V., Krivoruchko O.P., Isupova L.A. et al.* // Kataliz v promyshlennosti. 2017. Vol. 17. No. 5. P. 346.
17. *Buyanov R.A., Parmon V.N.* // Kataliz v promyshlennosti. 2017. Vol. 17. No. 5. P. 390.
18. *Zhuzhgov A.V., Krivoruchko O.P., Isupova L.A.* // Russ. J. Phys. Chem. 2020. Vol. 94. No. 1. P. 58.
19. *Boeva O., Antonov A., Zhavoronkova K.* // Catal. Comm. 2021. Vol. 148. P. 106173.
20. *Lu H.T., Li W., Miandoab E.S. et al.* // Front. Chem. Sci. Eng. 2021. Vol. 15. P. 464.
21. *Aasadni M., Mehrpooya M., Ghorbani B.* // J. Cleaner Production 2021. Vol. 278. P. 123872
22. *Wang C., Lui S., Lui L. et al.* // J. Mater. Chem. Phys. 2006. Vol. 96. P. 361.
23. *Casado P.G., Rasines I.* // J. Solid state Chem. 1984. Vol. 52. P. 187.
24. *Li W., Li J., Guo J.* // J. Eur. Ceram. Soc. 2003. Vol. 23. P. 2289.
25. *Fedotov M.A., Taraban E.A., Krivoruchko O.P. et al.* // Zh. neorg. khim. 1990. Vol. 35. No. 5. P. 1226.
26. *Bai C.S., Soled S., Dwight K.* // J. Solid State Chem. 1991. Vol. 91. P. 148.
27. *Fogg A.M., Williams G.R., Chester R. et al.* // J. Mater. Chem. 2004. Vol. 14. P. 2369.
28. *Williams G.R., Moorhouse S.J., Timothy J.P. et al.* // Dalton Trans. 2011. Vol. 40. P. 6012.
29. *Krivoruchko O.P., Buyanov R.A., Paramzin S.M. et al.*// Kinetika i kataliz. 1988. Vol. 29. No. 1. P. 252.
30. *Buyanov R.A., Krivoruchko O.P., Zolotovsky B.P.* // Izv. SB USSR AS. Ser. khim. nauk. 1986. No. 11. No. 4. P. 39.
31. *Ingram-Jones V.J., Davies R.C.T., Southern J.C. et al.* // J. Mat. Chem. 1996. Vol. 6. P. 73.
32. *Tanashev Yu.Yu., Moroz E.M., Isupova L.A. et al.* // Kinet. Catal. 2007. Vol. 48. No. 1. P. 153.
33. *Zhuzhgov A.V., Kruglyakov V.Y., Glazneva T.S. et al.* // Chemistry. 2022. V. 4. P.316.
34. *Zhuzhgov A.V., Kruglyakov V.Yu., Suprun E.A. et al.* // Russ. J. Appl. Chem. 2022. Vol. 95. No. 4. P. 512.
35. *Zhuzhgov A.V., Isupova L.A., Suprun E.A. et al.* // ChemEngineering. 2023. Vol. 7. N4. 71:1–16.
36. *Ivanova Y., Zhuzhgov A., Isupova L.* // Inorganic Chemistry Communications. 2024. Vol. 162. P. 1.
37. *Chukin G.D.* Structure of aluminum oxide and hydrodessulfurization catalysts. Mechanisms of reactions. Moscow: Paladin, Printa. 2010.
38. *Kosenko N.F.* // Izv. vysshykh uchebnykh zavedenii. 2011. Vol. 54. No. 5. P. 3.
39. *Krivoruchko O.P., Plyasova L.M., Zolotovskii B.P. et al.* // React. Kinet. Catal. Lett. 1983. Vol. 22. No. 3–5. P. 375.
40. *Van Nordstrand R.A., Hettinger W.P., Keith C.D.* // Nature. 1956. Vol. 177. P. 713.
41. *Shefer K.I., Cherepanova S.V., Moroz E.M. et al.* // J. Struct. Chem. 2010. Vol. 51. No. 1. P. 132.
42. *Danilevich V., Isupova L., Parmon V.* // Cleaner Engineering and Technology. 2021. Vol. 3. P. 1.
43. *Isupova L.A., Ivanova Yu.A.* // Dokl. Chem. 2023. Vol. 511. No. 2. P. 202.
44. *Lin H.K., Wang C.B., Chiu H.C. et al.* // Catal. Lett. 2023. Vol. 86. P. 63.